（11）EFFECT OF GRADED CARBON FIBER SHEET CONFIGURATION ON THE SEISMIC RETROFIT OF CIRCULAR STEEL BRIDGE PIERS

Kim Oliver U. MAGTAGÑOB[1], Hitoshi NAKAMURA[2] and Takahiro MATSUI[3]

[1]Member of JSCE, Student, Graduate School of Urban Environmental Sciences, Tokyo Metropolitan University
(1-1 Minami-Osawa, Hachioji, Tokyo 192-0397, Japan)
E-mail: magtagnob-kim-oliver-untalan@ed.tmu.ac.jp
[2]Member of JSCE, Associate Professor, Graduate School of Urban Environmental Sciences, Tokyo Metropolitan University (1-1 Minami-Osawa, Hachioji, Tokyo 192-0397, Japan)
E-mail: hnaka@tmu.ac.jp
[3]Member of JSCE, First Advanced Composites Technical Department, Toray Industries, Inc.
(2-1-1 Nihonbashi Muromachi, Chuo-ku, Tokyo 103-8666, Japan)
E-mail: Takahiro_Matsui@nts.toray.co.jp

In this study, the graded carbon fiber (CF) sheet configuration is proposed as a retrofit method for circular steel columns subjected to cyclic lateral loading and a constant axial force. The proposed graded carbon fiber sheet configuration optimizes circumferential CF sheet reinforcement by providing additional layers in the lower region of the columns where stress is concentrated. Two retrofitting methods were considered, first is the application of reinforcement before loading (reinforcement model) and the latter is the application of reinforcement after the specimen has undergone ultimate failure (repair model). Finite element analysis was performed to determine the optimum design for the proposed configuration. An experimental study is then conducted to further verify the effect of the graded configuration on the horizontal loading capacity, energy absorption, and buckling deformation of circular steel columns. It is concluded that the graded configuration can improve the ductility and strength of the steel columns for both reinforcement and repair models.

Key Words: *carbon fiber sheet, circular steel bridge pier, seismic retrofitting, elephant foot bulge*

1. INTRODUCTION

In Japan, the number of bridge structures reaching 50 years and older will double its current number in the next two decades. With the ever-increasing number of aging infrastructures, the need to repair and maintain these structures is becoming imperative. Because of its location in the Pacific Ring of Fire, the country experiences a high number of earthquakes which makes seismic resistance an important consideration in repair and maintenance. Reports on the damage of the Great Hanshin-Awaji Earthquake (1995) have shown that circular piers are prone to severe local buckling damage (elephant foot bulge) near its base[1), 2)]. Circular steel piers, due to their high strength and applicability on narrow sites, are commonly used in urban areas and damage to this structure can leave a huge impact after an event of a strong earthquake. Thus, an efficient seismic retrofitting method is needed for the emergency restoration of buckled steel piers. As a general seismic retrofitting method for existing steel piers, the concrete filling method and steel jacketing have been adopted. However, heavy machinery and long construction periods are needed for construction, and they do not have good workability considering the required working space and weight increase.

Carbon fiber (CF) sheet wrapping is being promoted as a seismic retrofitting method because CF sheets are lightweight, high-strength, and durable materials that are easy to install[3), 4)]. This material is widely used as one of the seismic reinforcement applications for concrete structures. However, it is hardly applied to steel structures. Experimental studies conducted on steel piers subjected to cyclic loading have shown that local buckling can be reduced by wrapping multiple layers of fiber reinforcements in the circumferential direction[5) - 8)]. It has been concluded that suppression of the plastic deformation results in improved toughness of test specimens. Moreover, it was found that the number and range of reinforcement influence the cyclic behavior and must be designed accordingly.

In addition, a study on the applicability of this method on the performance recovery of an already buckled specimen has shown that up to 90-95% of the bearing capacity before damage can be recovered[8)]. It has been clear that out-of-plane deformation of the already buckled specimen can be suppressed until the CF breaks.

In general, the reinforcement of steel columns with CF sheets has a positive effect on the loading capacity and energy absorption of the specimens. However, the constraining effect of CF reinforcements results in a diamond buckling mode (inward buckling) which drastically decreases the bearing capacity upon failure[5) - 8)].

In this study, the graded configuration of CF sheet reinforcement is proposed to improve the buckling deformation and delay the failure of circular steel piers subjected to constant vertical loading and static horizontal cyclic loading. The behavior of steel columns with graded thickness has shown positive improvements in strength, ductility as well as post-buckling deformation[9)]. The applicability of using varying thickness in the reinforcement of CF sheets and its effect on the seismic performance is examined in this study.

Initially, finite element analysis (FEA), which has been proven effective in reproducing hysteretic behavior of steel columns[10)], was used to select the optimum design of the number and range of CF layers of the proposed configuration. Then, an experimental study was carried out to confirm the seismic reinforcement effect of graded CF configuration. The efficiency of the retrofitting method was verified by comparing buckling deformation, horizontal loading capacity and the ultimate limit (point at which horizontal strength drops to 95% of peak and buckling is visually confirmed[11)]) of the specimens.

2. OUTLINE OF EXPERIMENT

(1) Circular steel specimen

In this study, a JIS STK400 grade steel (carbon steel tube for general structure) with a height of 1900 mm and an outer diameter of 457.2 mm was considered as shown in **Fig.1**. The material properties of the column specimen are summarized in **Table 1**. To prevent buckling near the base of the column, a section change from t_2 = 12.7 mm to t_1 = 9.5 mm is introduced at a position h = 300 mm from the base. In addition, stiffening ribs (12 pieces) with a height of 150 mm and a thickness of 16 mm are welded at the column base. The specimen was welded to a rigid steel plate with a thickness of 32 mm at the top and bottom to affix it to the base plates and the loading block jig. The specimen diameter-thickness ratio parameter R_t and the slenderness ratio parameter λ were designed to be within the applicable range ($0.03 \leq R_t \leq 0.08$, $0.2 \leq \lambda \leq 0.4$) stated in the Road Bridge Specification[12)] as shown in Eqs. (1) and (2).

$$R_t = \frac{R}{t}\frac{\sigma_y}{E}\sqrt{3(1-\nu^2)} \tag{1}$$

$$\lambda = \frac{2h}{\pi r}\sqrt{\frac{\sigma_y}{E}} \tag{2}$$

Here, R_t: radius thickness parameter, t: plate thickness, σ_y: yield stress, E_s: Young's modulus of steel, ν: Poisson's ratio of steel, h: effective buckling length, r: secondary radius of the cross-section. The yield stress (σ_y), Young's modulus (E_s), and Poisson's ratio (ν) of the steel were determined from the material tests on specimens cut from the circular steel specimen.

(2) Loading configuration

The test specimen is subjected to a constant vertical load to represent the superstructure weight which was set as 10% (492.9 kN) of the yielding axial force similar to the reference study[8)]. A gradually increasing cyclic horizontal loading is then applied at the top of the specimen by displacement control using the loading program shown in **Fig.2**. The positive loading side corresponds to the pulling direction of the horizontal loading jack whereas the are negative loading side is the pushing direction. The horizontal yield displacement (δ_y) was calculated using Eq (3) shown below.

$$\delta_y = \frac{H_y h^3}{3EI}, \text{where } H_y = \left(\sigma_y - \frac{P}{A}\right)\frac{S}{h} \tag{3}$$

Here, δ_y: horizontal yield displacement, H_y: horizontal yield load, h: loading height, EI: bending stiffness, σ_y: yield stress, P: axial force, A: cross-sectional area, and S: section modulus. The calculated yield horizontal displacement of the specimen is approximately 10 mm and a maximum of $\pm 9\delta_y$ was applied considering the maximum stroke of the test equipment. The dimensions of the specimen and the loading configuration are adopted from an existing experimental study[8)].

In this study, two cyclic loading programs were used depending on the type of retrofitting procedure: reinforcement and repair. The specimens for these two retrofitting

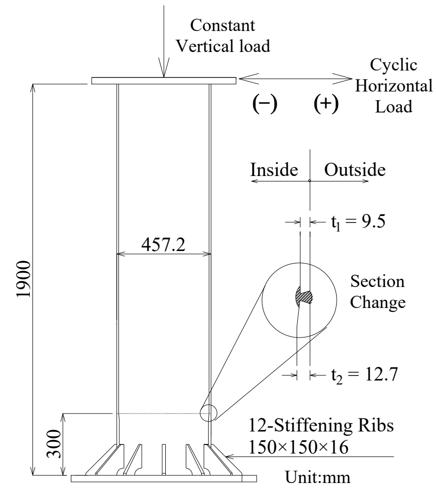

Fig.1 Schematic View of Test Specimen

Table 1 Material properties

Materials	Properties	Symbols	Units	Values
Steel Column (STK400)	Yield Stress	σ_y	MPa	368.9
	Elastic modulus	E_s	MPa	205,000
	D-t parameter	R_y	-	0.074
	Slenderness ratio	λ	-	0.328
CF sheet (UT70-30G)	Elastic modulus	E_{cf}	MPa	245,000
	Design thickness	t_{cf}	mm	0.167
	Poisson's ratio	ν_{cf}	-	0.2
Epoxy resin (AUP40T1)	Elastic modulus	E_m	MPa	3,430
	Thickness	ν_m	mm	0.38
CFRP	Fiber content	V_f	%	50
	Thickness	t_{cfrp}	mm	0.334
	Elastic modulus	E_l	MPa	111,800
	Elastic modulus	E_t	MPa	12,900
	Shear Modulus	G_{lt}	MPa	3,600
	Poisson's ratio	ν_{lt}	-	0.29

procedures will be referred to as (1) R - reinforced specimen and (2) S - repaired specimen.

For the reinforcement procedure, CF sheet bonding was performed on the circular steel specimen under no loads. Then, the vertical load and cyclic loading program shown in **Fig.2(a)** is applied. However, because of overheating issues in the horizontal loading jack during the experiment, loading was only completed until $\pm 8\delta_y$.

For the repair procedure, an unreinforced specimen was initially subjected to a primary loading, shown in **Fig.2(b)**, until the ultimate limit is reached. In this study, this condition was observed during the $\pm 6\delta_y$ cycle. After the primary loading, the horizontal jack was unloaded to 0 kN while the vertical load was maintained constant since it represents the superstructure weight. A residual displacement of approximately -35 mm was observed upon the unloading procedure which was maintained during the repair procedure. CF sheet bonding was then performed and secondary loading, shown in **Fig.2(b)**, was then applied to determine the strengthening effect of the CF sheet.

(3) Carbon fiber sheet reinforcement

High-strength CF sheets (UT70-30G) were used for the reinforcement and repair of the circular steel specimen. The reinforcements are applied, in circumferential direction, above the section change (h = 300 mm from the base) where buckling is expected to occur. The CF sheets are bonded to the specimen by vacuum-assisted resin transfer molding (VaRTM) method. Initially, bristle blasting was performed on the column specimen to remove the coating layer and produce a coarse surface. Next, to improve the bonding strength between the steel and the reinforcement, primer epoxy resin (E258R) was applied and was allowed to cure for 24 hours. Unevenness in the primer resin layer was then removed using a sander. The specimen is then covered with a chopped strand mat sheet followed by continuous wrapping of CF sheet. Sufficient tension was applied to minimize the wrinkles in the resulting CFRP. To ensure the restraining effect and prevent slippage, a lap length of 200 mm was provided at the start and endpoints. Peel ply and distribution media are then applied and the whole reinforcement area is covered with vacuum film. After applying vacuum pressure and performing leakage check, epoxy resin (AUP40T1) was injected. The CFRP was cured at 30 °C for at least 24 hours before loading conditions were applied. The properties of the reinforcement materials are shown in **Table 1**.

The graded configuration (R-G) of CF sheet reinforcement is proposed in this study to further improve the suppression of elephant foot bulge (EFB). Moreover, it optimizes the CF sheet reinforcement by increasing the range of reinforcement and providing more layers in the region where stress is concentrated. It is comprised of two segments of reinforcement: (I) thick CFRP layer and (II) thin CFRP layer. The former is from h = 300 mm to h = 450 mm whereas the latter is from h = 450 mm to h = 700 mm with fewer CF sheet layers as shown in **Fig.3(a)**. The range and number of sheets in R-G was determined considering the optimum uniform configuration (R-U) reinforcement. For the uniform configuration, a constant number of CF sheet layers are wound at a height of h = 300 mm to h = 600 mm from the base as shown in **Fig.3(b)**. The number of layers for the reinforcement configurations are determined by FEA.

3. SEISMIC DESIGN USING FINITE ELEMENT ANALYSIS

(1) Modeling of specimen

Finite element analysis was performed using the large strain nonlinear procedure of the general-purpose finite element program MSC Marc/Mentat 2019. The steel specimen and CFRP were modeled using 4-node thick shell elements as shown in **Fig.4**. The region within reinforcement was modeled using a mesh of 10 mm x 20 mm to accurately model the buckling while the other regions were modeled using a larger 20 mm x 20 mm mesh.

The steel was modeled as an isotropic elasto-plastic material with a kinematic hardening model of plasticity which can predict hysteretic behavior under cyclic loading with a relatively good accuracy[10)]. The true stress – true plastic strain plot obtained from the tensile tests was used to define the plasticity of steel. The CFRP was modeled as an elastic orthotropic material using the modulus obtained using the Halpin-Tsai model equations as shown in **Table 1**. Contact analysis option of FEA was then used to bond the steel and CFRP elements. The glued cohesive contact was used and perfect bonding between steel and CFRP was assumed.

For the boundary conditions, the displacements of all the nodes at the base of the specimen were restrained. A vertical load of 492.9 kN is applied at a node located at the top of the column model. The horizontal cyclic loading is

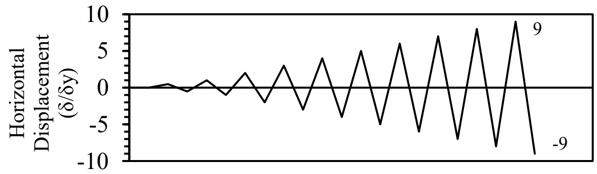

(a) Reinforcement

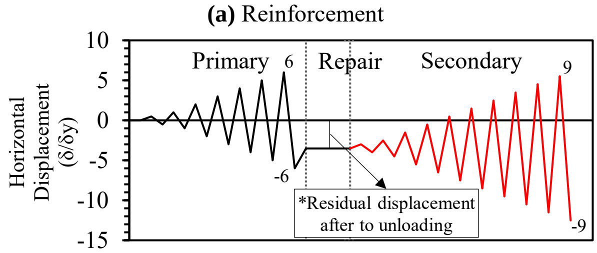

(b) Repair

Fig.2 Loading Program

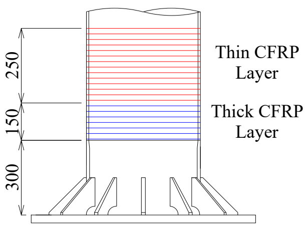

(a) Graded Configuration

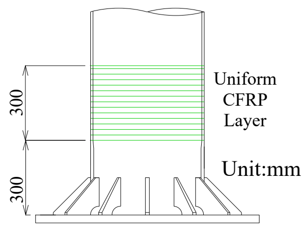

(b) Uniform Configuration

Fig.3 Reinforcement Configuration

also applied at the same node using the loading program shown in **Fig.2**.

(2) Design of reinforcement

Initially, the performance of uniform configuration under reinforcement loading program was examined using the finite element model (FEM) shown in **Fig.4(b)**. Varying number of CF sheet layers, from 1 to 10, was used for the analysis of uniform configuration. Moreover, a constant range of 300 mm, which was confirmed to be the optimal range[8)], was used for all R-U models. The envelope curves of the relationship between horizontal load and displacement of specimens with a uniform reinforcement of CF sheet are shown in **Fig.5**. It can be observed that an increase in the number of CF sheet reinforcements increases horizontal loading capacity and ductility. However, reinforcement beyond 9 layers of CF sheet results in over reinforcement of the section resulting in the occurrence of EFB above the reinforcement region at h = 650 mm from the base. Reinforcement of 9 layers of CF sheet provided an average increase of 15.72% on the horizontal loading capacity and provided twice the ductility performance of the unreinforced specimen based on the ductility factor. Hence, the R-U-9 model has been set as the basis for the selection of the graded configuration.

For the graded configuration (R-G), several combinations for the range and number of CF sheet layers. A parametric study was performed to determine the suitable combination for the range of segment I and segment II reinforcement. As seen in **Fig.3(a)**, the range of the thick CFRP layer is 150 mm. This is because of the expected stress concentration due to buckling deformation, as observed in the unreinforced model. For the thin CFRP layer, FEA was conducted to determine the sufficient range which is 250 mm. The number of layers of CF sheet was adjusted to satisfy the condition that the reinforcement volume of graded configuration models is at most the volume of R-U-9 reinforcement. The models discussed in this section and their corresponding maximum horizontal loads and ductility factor are summarized in **Table 2**. In addition, the CFRP ratio, which is calculated by dividing the reinforcement volume of the model by the reinforcement volume of R-U-9, for each model is also indicated.

The envelope curve of the graded configuration models is shown in **Fig.6** It can be seen that the proposed R-G models have similar performance with R-U-9 up to the $\pm 5\delta_y$ cycle. At this cycle, the R-U-9 model has reached its peak and local buckling already occurred resulting in a decrease in capacity in the succeeding cycles. Although the R-G models have higher horizontal loading capacities compared to R-U-9, the difference is considered insignificant and is limited to at most 4.08% increase on the uniform configuration.

The ductility factor ($\mu_{95} = \delta_{95}/\delta_y$, where δ_{95}: displacement at which peak horizontal load drops to 95%), on the other hand, has been improved by the R-G models with at most 16% higher ductility factor compared to R-U-9. R-G models reached the maximum horizontal loading at higher cycles resulting in a delayed failure as compared to R-U-9. However, R-G-12/3 was unable to improve the ductility

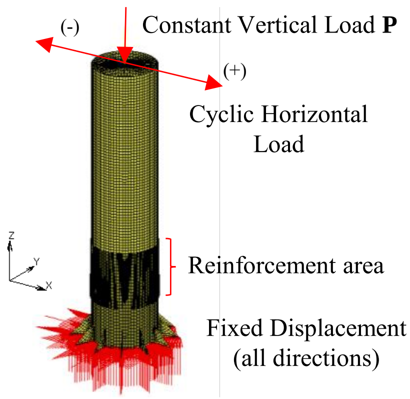

(a) Boundary Conditions

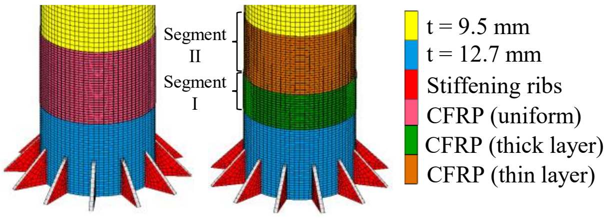

(b) R-U **(c)** R-G

Fig.4 Finite Element Model

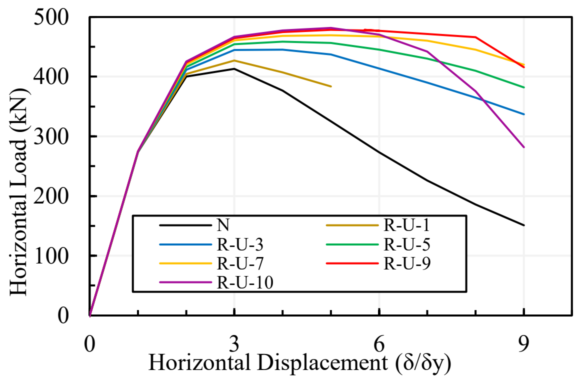

Fig.5 Envelope Curves for Uniform Configuration

Table 2 Summary of Analytical Results

Model*	CFRP Ratio	Maximum Horizontal Loads (kN)				Ductility Factor μ_{95}			
		(+) side	% inc.	(-) side	% inc.	(+) side	$\mu_{95}/\mu_{95\text{-}N}$	(-) side	$\mu_{95}/\mu_{95\text{-}N}$
N	-	413.2	-	- 411.6	-	4.2	1.00	-3.9	1.00
R-U-9	1.00	478.6	15.82	- 475.9	15.63	8.2	1.98	-7.9	2.03
R-G-9/5	0.96	488.7	18.27	- 486.8	18.27	8.4	2.02	-8.1	2.07
R-G-10/4	0.93	489.8	18.53	- 494.7	20.19	9.1	2.19	-8.2	2.11
R-G-11/4	0.98	493.4	19.40	- 498.1	21.03	9.2	2.21	-8.3	2.12
R-G-12/3	0.94	486.2	17.67	- 490.3	19.12	7.4	1.78	-7.0	1.78

*N: no reinforcement, R: reinforcement, U: uniform, G: graded configuration

*CF sheet layers are specified in the model name: R-G-(sheets at segment I)/(sheets at segment II) as seen in the sudden drop in capacity after ±7δ_y loading. It was observed that providing 3 layers in the thin CFRP layer is not enough and resulted in severe inward buckling as shown in **Fig.7**. The rest of the models provided better ductility performance than R-U-9 with R-G-10/4 and R-G-11/4 providing significant improvements.

The buckling deformation of the FEM is shown in **Fig.7**. Here, the deformation of the negative side of the column along the horizontal axis (x-axis in FEM) is plotted against height. The deformation was obtained at -8δ_y since the buckling is controlled by the reinforcement up to this point. For the N model, severe damage has already occurred and EFB phenomenon is visible. On the other hand, in the column reinforced using the uniform design (R-U-9), EFB is prevented but the constraining effect of CF sheet led to an inward buckling of about 20 mm from the out-of-plane direction of the column. R-G models, except R-G-12/3, provided a more controlled buckling deformation compared to R-U-9. R-G-10/4 and R-G-11/4 provided almost similar results and minimized the out-of-plane deformation to at most 5 mm. The deformation was distributed throughout the height of reinforcement with the maximum at h = 350 mm and a gradual decrease in deformation at higher heights. The minimal out-of-plane deformation in R-G-10/4 and R-G-11/4 resulted in better performance in both horizontal loading capacity and ductility performance. Because of the close behavior between the two models, the R-G-10/4 model that has a lower reinforcement ratio was selected as the reinforcement design for this study.

4. EXPERIMENTAL RESULTS AND DISCUSSION

(1) Buckling deformation and CFRP failure

Fig.8(a) shows the unreinforced specimen after the cyclic loading. An outward bulge developed at h = 350 mm to h = 450 mm from the base after the cyclic loading was unloaded. This bulging is more prominent on the negative side and was observed starting from -5δ_y loading. After the unloading of the horizontal jack, the buckling is about 10 mm in the out-of-plane direction of the column at h = 400 mm from the base.

Fig.8(b) shows the condition of the reinforced specimen after being subjected to cyclic loading (up to ±8δ_y). By visual inspection, no severe buckling deformation occurred and the graded CF sheet reinforcement suppressed the expected EFB condition that occurred in the unreinforced specimen. Based on the strain data, at -6δ_y loading, debonding occurred on the negative side at h = 400 mm and h = 500 mm from the base of the column. Debonding progressed on the negative side until the final loading and it was observed that at h = 350 mm to h = 450 mm from the base have debonded. In addition, a crack in the circumferential direction was observed at h = 400 mm on the negative side. The positive side underwent less damage and no debonding was observed. Crack initiation on the outermost layer of reinforcement was observed at h = 400 mm. Based on these results, most of the damage occurred in the thick region of reinforcement, and minimal damage was observed in the thin region which confirms that the 4 layers at h = 450 to h = 700 mm are sufficient.

Fig.9 shows the status of damage in the repaired specimen after the cyclic loading. During the ±2δ_y loading, debonding was observed at h = 350 mm and h = 450 mm on the negative side of the specimen. At ±6δ_y loading, debonding occurred at h = 350 mm and h = 400 mm on the positive side. A fracture sound was observed during -7δ_y loading and a huge crack was observed in the circumferential direction of the negative side of the specimen. At the final loading, severe damage occurred in the CFRP reinforcement at the range h = 350 to h = 400 mm from the base as seen in **Fig.9(b)**. The buckling that initially just occurred along the axis of loading has also propagated in the direction perpendicular to the axis of loading at a similar height. Similar to the reinforced specimen, the damage has been prominent at the range h = 300 mm to h = 450

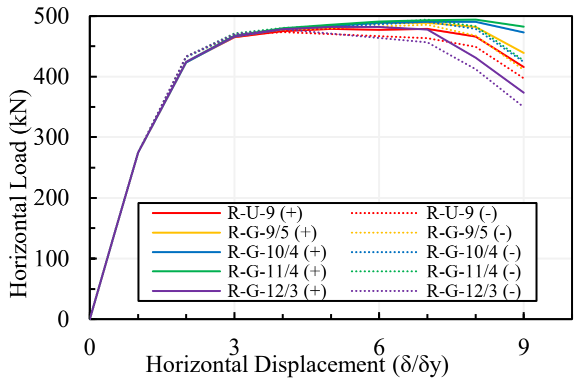

Fig.6 Envelope Curves for Graded Configuration

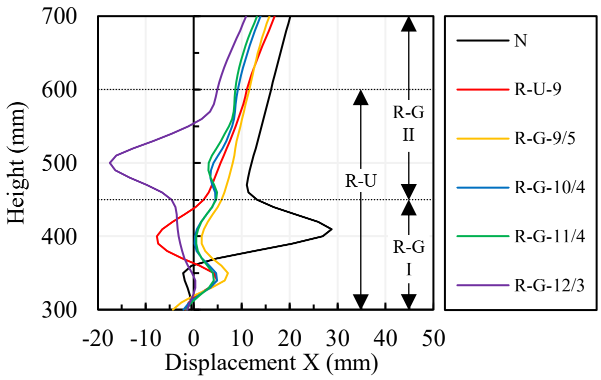

Fig.7 Buckling Deformation at +8δy Loading

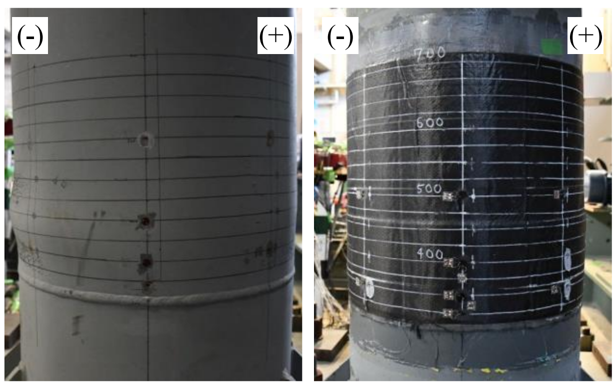

(a) N - Exp (at -6δ_y) **(b)** R - Exp (at -8δ_y)

Fig.8 Damage Status After Cyclic Loading mm from the base where the thick CFRP layer of the graded configuration was applied.

(2) Horizontal loading capacity and behavior of hysteresis loop

The relationship between the horizontal load and displacement is shown in **Fig.10** and the maximum horizontal loads for both positive and negative loading are shown in **Table 3**. In the unreinforced specimen, the maximum load is 404.94 kN (+5δ_y) for the positive loading side and -407.18 kN (-4δ_y) for the negative loading side. The behavior for the positive and negative loading sides are relatively similar until peak load. However, because of the progression of buckling on the negative side, the loading capacity was reduced to 90.8% (-6δ_y) of the peak for the negative side whereas the positive side was only reduced to 96.3% (+6δ_y) of the peak. Based on the previous study[8], a rapid decrease is expected beyond the ±6δ_y loading and bearing capacity is much lower than the ultimate limit beyond this loading. Hence, the N specimen is only loaded until ±6δ_y.

The hysteresis curve of the reinforced specimen is in **Fig.10 (a)** and the maximum load is 457.94 kN (+8δ_y) on the positive side and -450.79 kN (-7δ_y) on the negative side. This is a 15.6% and 10.7% increase on the maximum load for the positive and negative loading sides, respectively. After ±6δ_y loading, debonding initiated at the negative side of the column resulting in a minimal increase in capacity beyond this point. Similar to the unreinforced specimen, the negative side reached maximum load at an earlier cycle. At the final loading, a 1.7% decrease in peak was observed for the negative side, whereas no decrease was observed in the positive side. The results indicate that the reinforcement using the graded CF sheet configuration is effective in suppressing the buckling deformation. The behavior is also in agreement with the analytical results wherein the decrease in loading capacity after reaching peak load is very minimal.

Fig.10 (b) shows the hysteresis curve for the repaired specimen using the graded CF sheet design. The maximum horizontal loads for the repaired specimen are 442.23 kN (+7δ_y) on the positive side and -399.11 kN (-4δ_y) on the negative side. This shows that the repair by graded CF sheet configuration can recover the same level of performance before damage and can provide an increase of 9.22% loading capacity for the positive side. On the negative side, the maximum horizontal load obtained is 1.98% lower than that of the unreinforced specimen, which could be considered minimal. After the fracture of CFRP at -7δ_y, a decrease in capacity was observed in the succeeding cycles. During the final loading ±9δ_y, the loading capacity in the positive side was reduced to 75.7% while the negative side was reduced to 50.7%. The difference in capacity reduction at final loading is attributed to the initial buckling on the negative side and the residual displacement left after the unloading in the unreinforced test. This shows that higher displacements were applied on the negative side as compared to the positive side resulting in lower performance on the negative side. The results show that repair by graded CF sheet configuration can provide sufficient reinforcement to provide maximum loads similar to that of the unreinforced columns.

(3) Ductility performance and energy absorption rate

The ductility of the specimens was evaluated using the ductility factor ($\mu_{95} = \delta_{95}/\delta_y$) which corresponds to the displacement wherein the failure of the specimen was reached

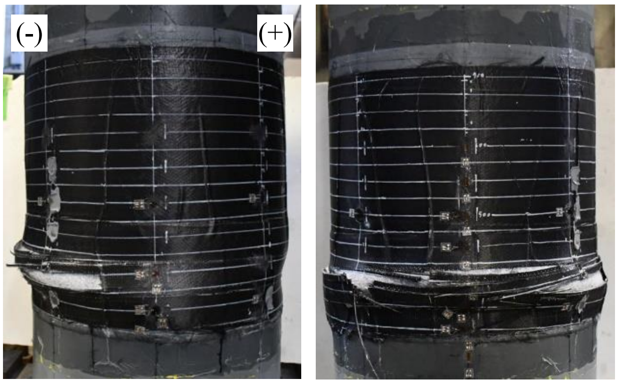

(a) Side View **(b)** Negative Loading Side

Fig.9 Damage of Repaired Specimen After Cyclic Loading

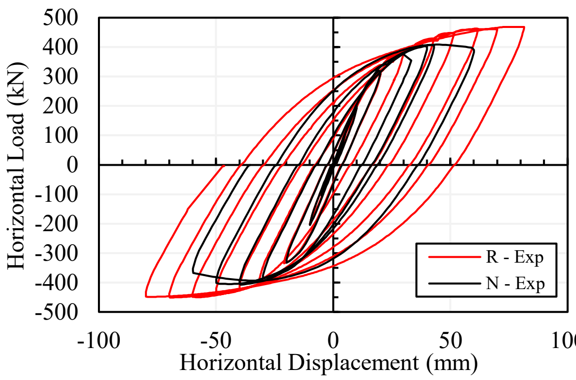

(a) Reinforced Specimen

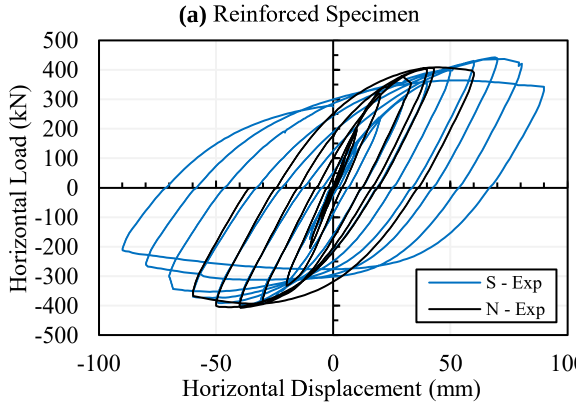

(b) Repaired Specimen

Fig.10 Load and Displacement Relationship

Table 3 Summary of Experimental Results

Model	Maximum Horizontal Loads (kN)		Ductility Factor μ_{95}		Energy Absorption Rate Against N	
	(+) side	(-) side	(+) side	(-) side	(+) side	(-) side
N - Exp	404.9 (+5δ_y)	- 407.2 (-4δ_y)	6.0	5.4	1.00	1.00
R - Exp	467.9 (+8δ_y)	- 450.8 (-7δ_y)	8.0	8.0	1.14	1.19
S - Exp	442.2 (+7δ_y)	- 399.1 (-4δ_y)	8.1	5.5	0.98	1.03

divided by the yield displacement. This is considered the ultimate limit and beyond this point, horizontal loading capacity drops significantly due to the progression of local buckling[11]. The ductility factors for the experiment are summarized in **Table 3**.

For the reinforced specimen, since failure was not reached during the cyclic loading, a ductility factor of 8.0 was used for both the positive and negative directions. It is found that there is an increase in ductility of more than 33.3% and 48.8% for the positive side and negative side, respectively. This difference in ductility performance can be attributed to the larger decrease in peak observed on the negative side of the unreinforced specimen which is not the case for the reinforced specimen. The graded CF sheet reinforcement is provided a more stable behavior and is effective in reinforcing circular steel pier specimens.

In the repaired specimen, an increase in the ductility performance of 34.4% was observed on the positive side. On the negative side, a minimal increase of 2.4% was observed. As mentioned previously, the repair was performed in a condition where residual displacement is present on the negative side. Nevertheless, the repair by graded CF sheet configuration was able to provide a similar ductility performance as the unreinforced specimen.

In addition, the performance recovery of test specimens was also evaluated using the energy absorption rate. The energy absorption rate was calculated by dividing the area under the envelope curves, until $\pm 8\delta_y$, of each specimen by the area of the unreinforced specimen envelope curve. Since the unreinforced specimen of this study was only loaded until $\pm 6\delta_y$, the area from the reference study[8] was used. The envelope curves are shown in **Fig.11** and the energy absorption rates are summarized in **Table 3**. The energy absorption rate for the reinforced specimen is about 14% higher in the positive direction and 19% higher in the negative direction than that of the unreinforced. Similar to the ductility factor discussed earlier, the higher rate observed on the negative side is attributed to the larger decrease in capacity after the peak observed on the negative side of the unreinforced specimen. For the repaired specimen, the positive side has an energy absorption rate of 97.8% while the negative side is higher by about 2.6% than that of the unreinforced specimen. For the positive side, the energy absorption rate is lower than the unreinforced from $\pm 1\delta_y$ to $\pm 4\delta_y$ but energy is recovered from $\pm 5\delta_y$ until final loading. Because of the negative residual displacement present in the repair procedure, lower displacements are actually applied on the positive side resulting in lower horizontal loads and energy absorption rates observed at the early cycles. Since the energy absorption rate of the positive side is only lower by 2.2% than the unreinforced specimen, it can be concluded that repair of a damaged specimen by graded CF sheet configuration can recover the performance of the unreinforced specimen.

The energy absorption rate was also compared to that of the reference study[8]. In the reference study, a uniform configuration with 7 layers of CF sheet and a range of 300 mm was used as a reinforcement and repair method. In addition, hand lay-up method, with an estimated 30% fiber content, was used as the bonding method of CF sheets in the said study. The summary of energy absorption rates for the reference study is shown in **Table 4**. In comparison, the energy absorption performance in the reinforcement procedure is almost similar to the reference study. However, a huge improvement can be observed in the repair procedure where the reference study failed to recover the performance of the unreinforced specimen. The graded CF sheet configuration used in this study provided an increase of 8.8% to that of the reference. In the reference study (S - Ref), a drop in capacity was observed after $-3\delta_y$ for the negative side and after $5\delta_y$ for the positive side. Whereas in the experimental results (S - Exp) using graded CF sheet configuration it was observed at $-4\delta_y$ and $7\delta_y$ for the negative and positive loading sides, respectively. This resulted in a higher reduction in capacity observed at the final loading of the reference study which affected the energy absorption capacity.

(4) Comparison with analytical results

Fig.11 shows the peak envelope curves obtained from the relationship between the horizontal load and horizontal displacement for the experimental and analytical results. It can be observed that the general behavior of the experimental and analytical envelope curves is in agreement. For the reinforcement, a steady behavior beyond peak was observed for both experiment and analysis. For repair, the envelope curve for the negative side is close to the envelope curve of the unreinforced specimen. On the positive side of repair, both analytical and experimental envelope curves are both initially below the curve of the unreinforced specimen and eventually become higher after several cycles. However, it can be seen that peak load and ultimate point for the experiment were achieved at lower loading cycles. This can be attributed to the limitations of the kinematic hardening plasticity model used in the FEA[10].

Table 4 Comparison of Energy Absorption Rate Against N of Reference Study[8]

Model	(+) Direction	(-) Direction
N - Ref	1.00	1.00
R - Ref	1.11	1.19
S - Ref	0.92	0.90

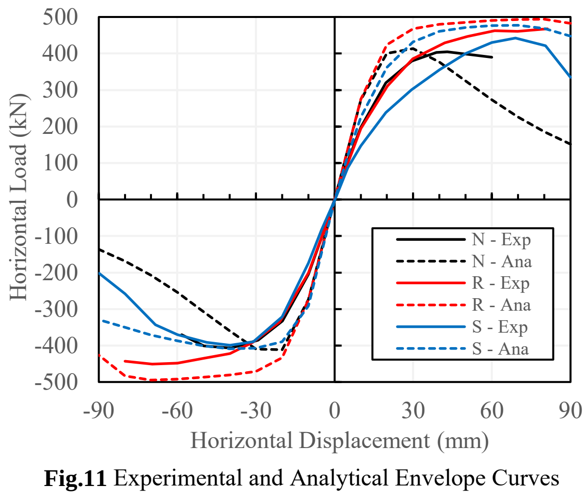

Fig.11 Experimental and Analytical Envelope Curves

Although a difference in the horizontal displacements at which maximum and ultimate points occurred was observed, the horizontal loading capacity was predicted to some extent. For the unreinforced specimen, a minimal 1.6% difference was observed between the experiment and analysis. However, for the reinforced and repaired specimens, higher percent differences of 7.3% and 5.0% were observed. Consequently, the increase in loading capacity due to the retrofit procedures was found to be also higher in the analysis than in the experiment. For the reinforcement procedure, an average increase of 19.80% was observed in the analysis and only 13.14% in the experiment. In the repair procedure, an increase of 7.39% and 3.62% for the reinforcement and repair procedures was observed, respectively. This is attributed to the conservative modeling of CFRP in the FEA. Since debonding and fracture of CFRP were not considered, the specimens were fully reinforced throughout the specimen in the FEA, which is not the case for the experiment, resulting in higher horizontal loading capacities in the analysis.

5. CONCLUSION

In this study, the graded carbon fiber sheet configuration is proposed as a seismic retrofitting method for circular steel specimens. The results obtained are shown below.

(1) In the reinforcement using the graded carbon fiber sheet configuration, severe out-of-plane deformation was prevented resulting in an average increase of 13.4% horizontal loading capacity. The ductility performance was increased by an average of 41.1% and it was found that the effect varies depending on the direction of loading.

(2) In the repair using the graded carbon fiber sheet configuration, the initial buckling deformation was maintained until the failure and debonding of the carbon fiber sheets. The horizontal loading capacity after repair can recover at least 98% to that of the non-damaged specimen. The ductility performance can be fully recovered by repair with an improvement of 34.4% on the positive side.

(3) In comparison with a reference study that uses uniform configuration reinforcement, the graded CF sheet configuration provided similar energy absorption performance for the reinforcement procedure but improved the energy absorption performance for the repair procedure.

(4) The finite element modeling using the kinematic hardening constitutive model and the plasticity behavior obtained from tensile tests can provide the loading capacity for all specimens which are in agreement with the experiment. However, the modeling used does not provide an accurate representation of the load and displacement relationship observed in the experiments.

As future work, further analysis will be performed to provide a better agreement between analytical and experimental results. In addition, the failure and debonding of the reinforcement, which influences the relationship between the horizontal load and horizontal displacement, will be studied and incorporated in the design stage.

REFERENCES

1) Hanshin Expressway Management Technology Center: Overcoming the Great East Japan Earthquake, Recovery Construction Magazine, Hanshin Expressway Public Corporation, 1997.
2) Bruneau, M.: Performance of steel bridges during the 1995 Hyogoken-Nanbu (Kobe, Japan) earthquake—a north American perspective, *Engineering Structures*, Vol.20, No.12, pp. 1063-1078, 1998.
3) Concrete Engineering Committee of the Japan Society of Civil Engineers: Guidelines for repair and reinforcement of concrete structures using continuous fiber sheets, Concrete Library 101, 2000.
4) (Foundation) Public Works Research Center: Retrofit guidelines of the steel piers by carbon fiber sheet (draft), 2002.7
5) Watanabe, T., Ishida, K., Hayashi, K., Yamaguchi, T., Ikeda, N.: Seismic reinforcement of steel bridge piers using a carbon fiber sheet, *Journal of Structural Engineering*, Vol.48A, pp. 725-734, 2002.3
6) Matsumura, M., Kitada, T., Tokubayashi, M., Ikeda, K., Okada, T.: Experimental study on seismic retrofitting of steel pier columns with carbon fiber sheets attached circumferentially, *Proceedings of the Japan Society of Civil Engineers*, No.766/ I-68, pp. 17-31, 2004.7
7) Komuro, M., Kishi, T., Mikami, H., Nishi, H.: AFRP sheet wrapped around the static loading tests on seismic reinforcement of the real scale steel pipe piers by, *Journal of Structural Engineering*, Vol.52A, pp. 1327-1336, 2006.3
8) Okazaki, N., Nakamura, K., Kishi, K., Matsui, T., Setouchi, H.: Study on performance recovery of buckling damaged circular steel piers by rolling up carbon fiber sheet, *Journal of Japan Society of Civil Engineers A1 (Structure and Earthquake Engineering)*, Vol.73, No.1, pp. 69-83, 2017.5
9) Al-Kaseasbeh, Q., Mamaghani, I.: Buckling strength and buckling strength and ductility evaluation of thin-walled steel tubular columns with uniform and graded thickness under cyclic loading, *Journal of Bridge Engineering (American Society of Civil Engineering)*, Vol.24, No.1, pp. 04018105-1-12, 2019.1.
10) Goto, Y., Wang, K., Takahashi, N., Obata, M.: Analysis of steel piers under cyclic loading by finite element method and material constitutive law, *Journal of Japan Society of Civil Engineers*, No.591, I-43, pp. 189-206, 1998.
11) Chen, S., Xie, X., Zhuge, H.: Hysteretic model for steel piers considering local buckling of steel plates, *Engineering Structures*, Vol. 183, pp. 303-318, 2019.
12) Japan Road Association: Specifications for Road Bridges, Commentary, (1) Seismic Design, pp. 225-230, 2012.

(Received September 10, 2021)